



Scale-independent shape analysis for quantitative cytology using mathematical morphology

Volker Metzler^{a,*}, Thomas Lehmann^b, Hans Bienert^c, Khosrow Mottaghy^d,
Klaus Spitzer^b

^a*Institute for Signal Processing, Medical University of Lübeck, Ratzeburger Allee 160, D-23538, Lübeck, Germany*

^b*Institute of Medical Informatics, Aachen University of Technology, Germany*

^c*Interdisciplinary Center for Clinical Research on Biomaterials, Aachen University of Technology, Germany*

^d*Institute of Physiology, Aachen University of Technology, Germany*

Received 8 October 1998; accepted 16 December 1999

Abstract

A system for automatic quantification of morphological changes of cell lines, proposed for cytotoxicity tests of biomaterials, is presented. Light-micrographs of cultured cells are segmented by adaptive thresholding within a local adaptive window. Connected cells in binarized micrographs are separated by a novel morphological multiscale method, treating cells in their size-specific scale and hence resulting in scale-independent separations. Significant shape descriptors correlating well with cell toxicity are extracted from single cells. Size and compactness distributions turned out to be reliable and useful parameters, providing an alternative to the common subjective grading of shape deformations by visual inspection. The system is evaluated for several standardized toxic reference substances and is now in use for clinical biocompatibility testing. © 2000 Elsevier Science Ltd. All rights reserved.

Keywords: Shape analysis; Segmentation; Mathematical morphology; Scale-space; Computer-assisted microscopy; Quantitative cytology

1. Introduction

Biocompatibility is the most important requirement for the development of medical devices.

* Corresponding author. Tel.: +49-451-3909-559; fax: +49-451-3909-555.

E-mail address: metzler@isip.mu-luebeck.de (V. Metzler).

To prevent toxic effects on humans following the implantation of synthetic prostheses or artificial organs, extensive toxicity tests are mandatory to evaluate the impact of new or modified materials. Morphological changes of standard cell lines cultured on these biomaterials indicate toxicity. They can be related to pathological effects caused by the biomaterial. However, cytotoxicity studies are currently limited to qualitative or semi-quantitative analysis, based on visual inspection of stained microscopic samples and subsequent interactive measurements of relevant features.

Cellular toxicity finally leads to changes in morphology. It is safe to assume that toxic effects on vital cells result in a rounding, shrinking, and defacing of cells, which are otherwise more extended and have differentiated contours [1]. Currently, the evaluation of cytotoxicity by means of microscopic observation of cell deformation is qualitative and the effects can be recorded only descriptively as deviations from normal cell morphology. This causes the well-known ambiguities in interpretation and comparison of different biological studies.

Fortunately, an increase in computational power, combined with advanced staining techniques from molecular biology has recently led to computer-assisted examination of relevant image features in microscopic samples [2,3]. The spatial frequencies of micrographs thus can be used to extract information on distances between cells and their position in the image. However, such information is less useful in quantitative cytology. Instead, the structural analysis of cell populations is often performed by methods of mathematical morphology [4,5], particularly by morphological filters for their shape — rather than frequency-oriented operations [6]. These versatile tools can be used at different stages of the automated feature quantification process such as preprocessing [7], segmentation [8], and feature extraction [9]. Furthermore, shape descriptors for binary objects and methods for separating connected objects have been proposed [5,10,11].

Unfortunately, such benefits from modern technologies are not established in medical routine yet. For example, deformations of naturally shaped fibroblasts, which represent a standard cell line for cytotoxicity studies, are still determined by visual inspection. In this paper we report a method to extract reproducible morphological cytotoxicity data of biomaterials by automatic shape analysis and quantitatively evaluate populations of standard cell lines. For this, the analysis of digitized micrographs is performed in three stages: (i) segmentation; (ii) separation; and (iii) quantification.

Generally speaking, image segmentation is the first and most important step in image analysis or pattern recognition systems. Several segmentation and interpretation techniques have been developed [8,12,13], from which only a few are useful in digital cytological imaging [14–17]. This is due to the numerous problems that arise from variances in illumination, layer thickness, or dye concentration. In an attempt to compensate such problems, we introduce a local adaptive thresholding technique estimating thresholds and window sizes from local graylevel distributions (Section 2.1). Since the size and shape of cells may differ, a morphological multiscale approach is used to separate connected cells [18,19]. Initially, the image is decomposed into size-specific scales of distinct morphological markers, each of which indicate the presence of one cell without dealing with its shape. The converse synthesis of scales reconstructs the cells and prevents merging of already separated objects (Section 2.2). This process results in scale-independent separations, because differently sized cells are treated within their proper scale. The subsequent extraction of characteristic features of cells such as

size, perimeter, and compactness, provides quantitative parameters of their distributions (Section 2.3). These parameters for cytotoxicity were found to be significant for the different toxicity levels of a standard cell line (mouse fibroblasts) subjected to defined concentrations of several toxic reference substances (Section 3).

2. Automatic shape analysis

2.1. Segmentation of micrographs

Segmentation means partitioning an image into non-overlapping regions corresponding to the interpretation of human observers [20]. With respect to a population of fibroblasts, segmentation is supposed to yield two regions: cells and image background.

Typically, graylevels occurring within objects differ significantly from those in the background. This results in a bimodal histogram function, which can be split into two parts by a global threshold. If all objects were of equal graylevel characteristics (i.e. the cells are of the same type), a histogram thresholding technique may be applied as long as the background appears homogeneous.

Unfortunately, on light micrographs of cytological samples, illumination and dye concentration may vary significantly (Fig. 1, *upper left*). Moreover, in many cases the thickness of the specimen, and hence its translucence, cannot be assumed to be constant. This leads to poor segmentation results by global thresholding (Fig. 1, *upper right*).

Unlike other approaches that primarily aim to remove the low-frequency illumination component from the images [21,22], we use a local thresholding technique that is directly applied to the image. However, if the distribution of objects in the image is not homogeneous,

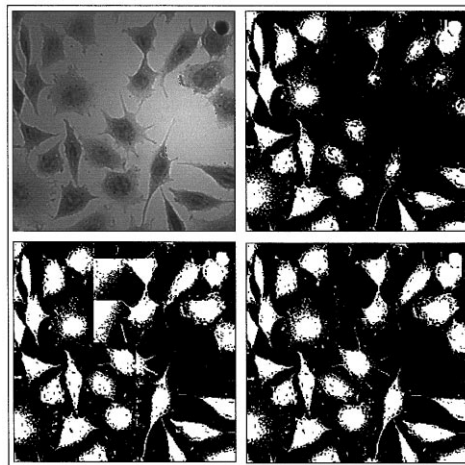


Fig. 1. The cytological sample (*upper left*) shows connected and inhomogeneously distributed cells. Global histogram thresholding (*upper right*) and local thresholds of constant window size (*lower right*) do not lead to acceptable results. Results are improved by local adaptive threshold windows (*lower left*).

local thresholding with constant window sizes also causes problems (Fig. 1, *lower left*). The rectangular artifacts result from a too small window size. Increasing the window size, however, would produce similar binarization errors as provoked with global thresholds.

For optimal thresholding results, window sizes need to be adapted to local graylevel distributions in the image. Large graylevel variances require small window sizes and vice versa. The local window size is determined iteratively. Starting with a small window surrounding the point of interest, the variance of graylevels is compared to the entire image's variance. As long as the local variance stays below the global one, the window size increases. Strictly speaking, a local window is determined as the smallest window with a variance that indicates the presence of different regions. In principle, any kind of thresholding technique may be applied within the local adaptive window to group the window's center pixel to the object or to the background. For the segmentation of fibroblast populations the histogram thresholding technique proposed by Otsu was chosen [23]. This threshold maximizes inter-class and minimizes intra-class variance, respectively (Fig. 1, *lower right*).

2.2. Object separation by mathematical morphology

Below, we describe the algorithms used to separate connected cells under noisy conditions. A brief introduction to morphological reconstruction is given; for further details, see [5,24].

2.2.1. Morphological reconstruction filters

Reconstruction filters are based on the elementary dual filters n -fold erosion $\mathbf{E}_\sigma^n(B)$ and n -fold dilation $\mathbf{D}_\sigma^n(B)$, which represent the local minima and maxima of the binary image B in a region, respectively. The region is determined by a circular binary structuring element specified by its radius σ . The n -fold masked erosion $\mathbf{E}_\sigma^n(B, M)$ and dilation $\mathbf{D}_\sigma^n(B, M)$ additionally require a binary masking image M , which marks the manipulable pixels of B . Masked operators lead to white-reconstruction $\mathbf{D}_\sigma^\infty(B, M)$ and black-reconstruction $\mathbf{E}_\sigma^\infty(B, M)$ by iteratively performing a masked morphological operation until B reaches a steady state (denoted by ∞). M is reconstructed by expanding the initially smaller objects of B .

The dual operators white-skiz $\mathbf{D}_\sigma^{\text{skiz}}(B, M)$ (skeleton-by-influence-zone) and black-skiz $\mathbf{E}_\sigma^{\text{skiz}}(B, M)$ differ from the above reconstruction operators by prohibiting the merge of separated markers [8]. This results in a one-pixel gap between those objects in B that are already covered by the same object in M . Therefore, the number of objects in $\mathbf{D}_\sigma^{\text{skiz}}(B, M)$ equals those in B . Basically, the white-skiz is the skeleton of the background and can be regarded as a binary analogon of the watershed transform for graylevel images [25].

The (n -fold) opening $\mathbf{O}_\sigma^n(B) := \mathbf{D}_\sigma^n(\mathbf{E}_\sigma^n(B))$ and closing $\mathbf{C}_\sigma^n(B) := \mathbf{E}_\sigma^n(\mathbf{D}_\sigma^n(B))$ are compositions of erosion and dilation. The reconstructive opening/closing [24]

$$n\text{-opening by reconstruction: } \mathbf{O}_\sigma^{(n, \infty)}(B, M) := \mathbf{D}_\sigma^\infty(\mathbf{E}_\sigma^n(B), M) \quad (1)$$

$$n\text{-closing by reconstruction: } \mathbf{C}_\sigma^{(n, \infty)}(B, M) := \mathbf{E}_\sigma^\infty(\mathbf{D}_\sigma^n(B), M) \quad (2)$$

reconstructs M from B after noise filtering by the corresponding dual filter. For $M=B$, these filters perform a nonlinear noise reduction preserving object boundaries by removing

compartments smaller than the n times iterated operator σ . In contrast to non-reconstructive n -fold opening and closing, object boundaries are not smoothed. Complementary effects of both filters can be combined by their successive application. For example, the

$$n\text{-double reconstruction filter: } \Psi_{\sigma}^{(n,\infty)}(B) := \mathbf{C}_{\sigma}^{(n,\infty)}(\mathbf{O}_{\sigma}^{(n,\infty)}(B,B),B) \quad (3)$$

removes both white and black compartments from B .

2.2.2. Noise filtering

Binarized samples are always noisy because of detection errors, cell particles, or other artifacts. Digitization and quantization introduce additional noise, which must be removed while the information to be quantified must be preserved.

Classification of binary segments into cells and noise is done with respect to the absolute size of these segments. The digital images (in 100 times microscopical magnification) display an area of $422.4 \times 607.3 \mu\text{m}$ covering in total 0.256 mm^2 . Filtering is performed by a double reconstruction filter of size $\sigma = 3$ [Eq. (3)], which is approximately $2.4 \mu\text{m}$. This filter removes circular objects of area $24.5 \mu\text{m}^2$ or ellipsoidal objects, with at least one axis smaller than $4 \mu\text{m}$. These values are well below the expected minimal area of totally damaged and rounded fibroblasts.

2.2.3. Multiscale separation

The working hypothesis for binary object separation is that connected cells can be best separated to yield distinct markers within their size-specific scale. The cells can be progressively segmented by reconstructing them from previously found markers [8]. The reconstruction algorithm proposed here has two stages. The *analysis stage* decomposes an image into marker scales B_i obtained by *enhanced erosion*. This yields a distinct marker for each cell. The subsequent *synthesis stage* reconstructs the original shapes B_0 , from the multiscale representation B_i using *enhanced dilation*, while preventing already separated markers from merging again (Fig. 2).

2.2.3.1. Analysis by enhanced erosion. The binary image B_i represents the markers at scale $0 \leq i < I \in \mathbb{N}$, where I is the total number of scales. The complete scale-space is generated by a cascade of I successive enhanced erosions (Fig. 3)

$$B_{i+1} = \mathbf{D}_{\sigma}^m(B_i'', B_i') \quad \text{with} \quad B_i' = \mathbf{E}_{\sigma}^1(B_i) \quad \text{and} \quad B_i'' = \mathbf{E}_{\sigma}^n(B_i) \quad (4)$$

where \mathbf{D}_{σ}^m and \mathbf{E}_{σ}^n denote m -fold dilation and n -fold erosion, respectively. $\mathbf{D}(B, M)$ denotes the masked dilation (Section 2.2.1). At scale i , the n -eroded image B_i is m -dilated and masked by the 1-eroded B_i , resulting in the next scale image B_{i+1} . Each of these scale images introduces separations of those cells belonging to that specific scale.

The parameters n and m are derived from the estimation described in Section 2.2.2. Likewise initial n -double reconstruction, the n -fold erosion filters false markers and for this $n = 3$ is appropriate for all scales. Eq. (4) actually represents an opening. Hence $m > n$ is an initial constraint for the m -fold dilation. For $m = n$ the number of false markers is too large. The $(m = n + 1)$ -dilation turned out to be a good compromise between the generation of false

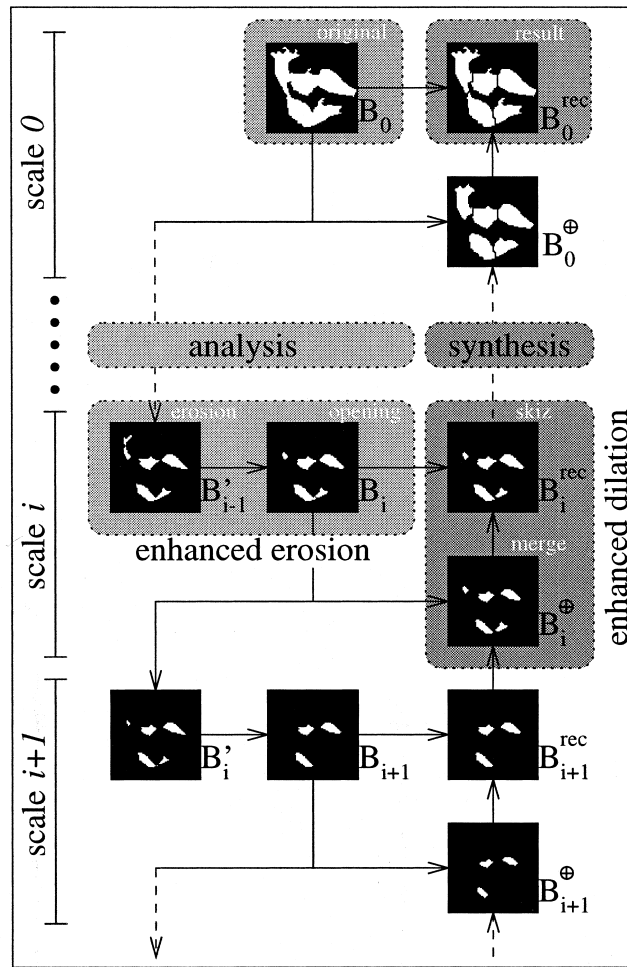


Fig. 2. Scheme of the two-stage multiscale separation procedure. The analysis extracts separated markers for the cells by *enhanced erosion*. During converse synthesis the *enhanced dilation* operator reconstructs the original cell shapes preventing the merge of separate markers.

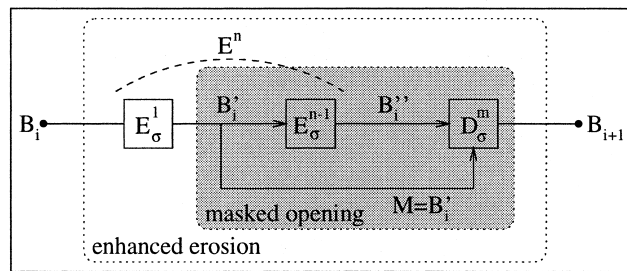


Fig. 3. Enhanced erosion is basically an opening operation consisting of n -erosion and masked m -dilation. Since the constraint $m=n + 1$ proved useful, the operator is controlled by n , which exclusively depends on the minimum cell size [Eq. (4)].

markers and the correct separations of different cells. The total number of scales is a rather uncritical parameter, as long as it is above a certain threshold depending on the maximum size of the cells. For the separation of fibroblasts at magnification 100, a scale–space of $I = 12$ is sufficient. The values of the control parameters n and I depend exclusively on the size of cells and hence can be determined automatically prior to separation.

2.2.3.2. *Synthesis by enhanced dilation.* The synthesis of marker scales B_i reconstructs the original cell shapes of B_0 . At each scale i a reconstructed image B_i^{rec} is calculated, which incorporates the marker information of all scales $j \geq i$ and hence preserves their separations. These markers are reconstructed to the object size of scale i by combining B_{i+1}^{rec} and B_i such that $B_i \supseteq B_{i+1}^{\text{rec}}$. Therefore, the resulting image B_i^\oplus consists of all markers of B_{i+1}^{rec} plus those occurring in B_i , but not in B_{i+1}^{rec} :

$$B_i^\oplus = B_{i+1}^{\text{rec}} \cup \{B_i \setminus B_{i+1}^{\text{rec}}\}. \tag{5}$$

This procedure ensures that no separation is lost during synthesis. The various inclusion relations between intermediate steps in multiscale deagglomeration are illustrated in Fig. 4. Finally, a white-skiz reconstruction is applied to extend the shapes of B_i^\oplus to those of B_i preserving their separations (Section 2.2.1). This yields B_i^{rec} , i.e. the reconstructed markers of scale i :

$$B_i^{\text{rec}} = \mathbf{D}_\sigma^{\text{skiz}}(B_i^\oplus, B_i). \tag{6}$$

We compared the algorithm with two common separation techniques considering both synthetic and natural images (Fig. 5). The separations shown in the *second column* of Fig. 5 were obtained by Serra’s algorithm, which considers each ultimate eroded point of a binary set as

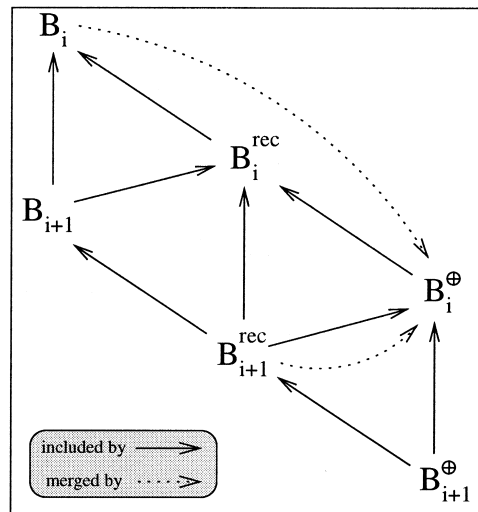


Fig. 4. The various intermediate marker images, which are generated during multiscale separation are related by inclusion. From a set-theoretic point of view, these images form a partial ordering.

the center of an individual object [10]. The separation lines between the objects are determined to have maximal distance from all adjacent ultimate eroded points. Two disadvantages are obvious: (i) all objects have to be of similar size; and (ii) all objects must exhibit regular shapes. Compact objects of different size (Fig. 5, *upper row*) cannot be separated correctly because the marker generation depends on size and scale. The number of markers, however, is correct in most cases. Objects with irregular shapes (Fig. 5, *lower row*) produce too many markers because the geometric interpretation is drawn from one single scale. This results in oversegmented images. Fig. 5 (*third column*) shows the separation results obtained by reconstructing the maxima of the distance transform [26,27]. Although the distance transform is able to handle differently sized objects, irregularly shaped cells still cause oversegmentation. Our two-stage multiscale approach avoids these drawbacks of common separation techniques, which result mainly from the single-scale nature of the previous algorithms. Generation of a morphological scale-space, filtering of false markers, and their stepwise reconstruction is independent of the object's size and notably improve results (Fig. 5, *fourth column*).

2.3. Quantification of shape descriptors

To determine exact shape descriptors from digital images, transitions from analog to digital objects and expression of complex shape characteristics by real feature vectors must be considered.

Using CCD cameras, differences between lengths of continuous and discrete contours decrease on increasing resolution [11]. Reasonably small deviations between analog and digital lengths are obtained by using an indirect neighborhood with diagonal lengths corrected by the factor $\sqrt{2}$ [28].

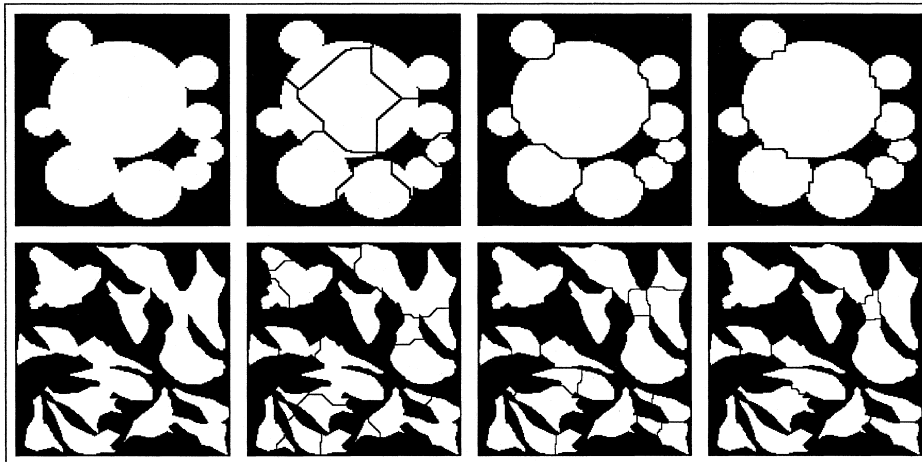


Fig. 5. Synthetic image (*upper row*) and binarized micrograph (*lower row*) showing objects to be separated. Both separations, the reconstruction of filtered ultimate eroded points (*second column*) and the reconstruction of filtered maxima of the distance transform (*third column*) yield poor results. Our multiscale separation algorithm yields good results for synthetic images and performs best for cell micrographs (*fourth column*).

Besides color, shape is the most important feature to assess the condition of cytological structures. Among existing similarity measures for graylevel images [29], only a few are applicable for binary images [11]. One major requirement for a comprehensive shape parameter is rotation and translation invariance. Furthermore, it is not sufficient to measure only the elongation of an object (as done by the *aspect ratio*). Since shape irregularities are most valuable characteristics to quantify cytotoxicity, the *compactness* C of binary objects appears to be an appropriate parameter:

$$C = \frac{4\pi \text{ area}}{\text{perimeter}^2} \quad \text{with} \quad 0 \leq C \leq 1. \quad (7)$$

This measure estimates shape irregularities and is rotation invariant. The number of inflection points of an object's contour might also be a useful parameter, but its computation is far more expensive.

3. Application and results

The proposed method has been evaluated for fibroblast cells treated with three different toxic reference substances: ethanol, and the two toxic polymers SRMA and SRMB (standard reference materials A and B). During all experiments, geometric analysis was performed with external parameters set to $n = 3$, $m = 4$, and $I = 12$ [Section 2.2.3, Eq. (4)].

3.1. Ethanol

Three large populations of fibroblasts (268 images each), in contact with 0, 5, and 10% concentration of ethanol, respectively, were collected; 10% ethanol concentration causes a complete destruction of cells. They round and shrink in size. The experimental setup is described in [17].

Since the compactness is not normally distributed (it is limited to the range [0;1]), a Wilcoxon two-sample test (calculated by SAS v12.6) was used to decide whether the obtained distributions differ significantly. Altogether, 29,939 cells ($\mu=0.465$, $\sigma=0.2$), 19,801 cells ($\mu=0.514$, $\sigma=0.236$), and 10,495 cells ($\mu=0.711$, $\sigma=0.259$) were detected for 0, 5, and 10%, respectively. For all pairs of ethanol concentrations (0 versus 5%, 0 versus 10%, and 5 versus 10%) the hypothesis of equal distributions can be rejected ($p < 0.0001$). Therefore, the compactness distribution of a cell population is an appropriate indicator of toxicity. This result is emphasized by the scatter diagrams in Fig. 6, which show relation of size (x -axis) and perimeter (y -axis) of 500 arbitrarily chosen cells. Both size and perimeter decrease monotonously for increasing toxicity. Also, the centers of gravity of the clusters are shifting towards more compact objects on increasing ethanol concentration.

The inserted table gives a set of automatically determined parameters, each of which indicate morphological changes by monotonous behavior. Despite the coverage, all parameters require the separation of agglomerated cells. One has to discriminate between those parameters depending on the number of cells in the population (density, coverage) and the normalized

parameters. In this experiment, density and coverage also yield good discrimination among different toxicities, since they reduce approximately to 60 and 10% for 5 and 10% ethanol concentration, respectively. However, more objective quantifications of actual shapes are given by those parameters which are independent of the cell number, because they represent geometrical features only.

3.2. SRMA and SRMB

SRMA and SRMB are toxic polymers with different toxicity. Both standard reference materials are made of polyurethane films containing various amounts of cytotoxic compounds [30]. All polymers, including the nontoxic control polymers (negative reference), were extracted under standard conditions (2 cm² polymer/ml cell culture, time 72 h, temperature 37°C). Extracts were then diluted to show dose dependent morphological changes to the fibroblasts that are basically the same as for ethanol. For both substances a negative reference population showing completely vital cells and a positive reference population showing completely damaged and deformed cells exemplify the cytotoxic extremes.

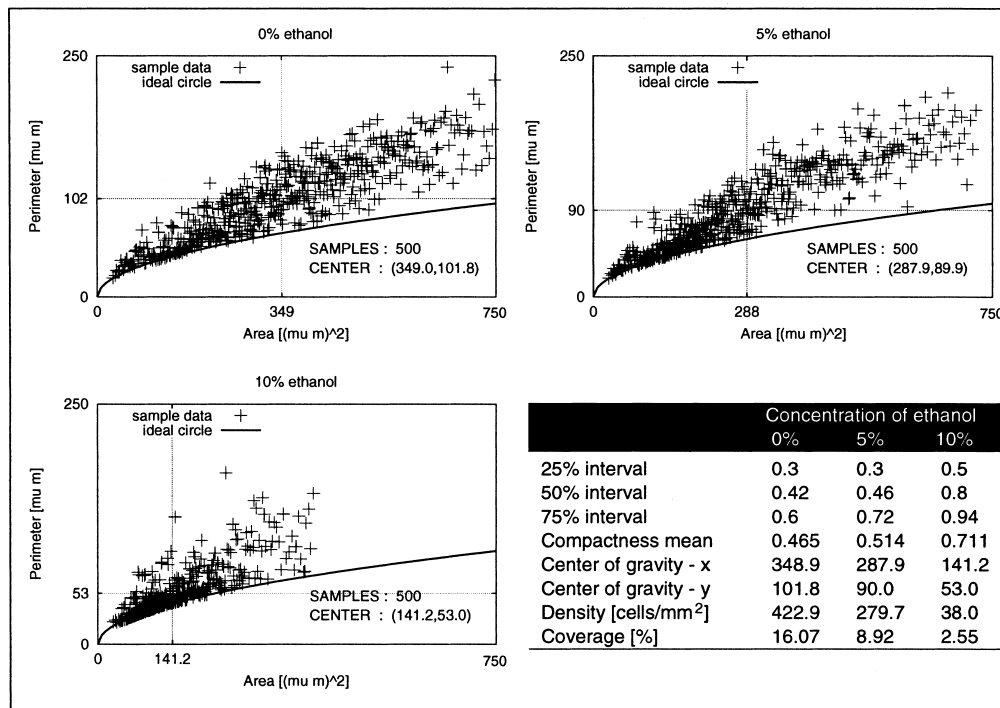


Fig. 6. Results of cytotoxicity tests with fibroblasts in 0% (upper left), 5% (upper right), and 10% ethanol (lower left). These diagrams show 500 arbitrarily chosen cells with their covered area on the x-axis and perimeter on the y-axis. The center of gravity is marked in each scatter plot. The table shows all extracted quantitative parameters for each of the three distributions (lower right).

Since SMRA is more toxic than SRMB, the SRMA toxicity was tested for 10 and 20% concentration, while SRMB was tested for concentrations of 50 and 100%. For both substances the compactness distributions were found to differ significantly by a Wilcoxon two-sample test.

The four SRMA distributions “negative” (5128 cells, $\mu=0.587$, $\sigma=0.172$), 10% (3857 cells, $\mu=0.689$, $\sigma=0.169$), 20% (1901 cells, $\mu=0.731$, $\sigma=0.181$), and “positive” (2226 cells, $\mu=0.801$, $\sigma=0.165$) differ significantly ($p < 0.0001$).

Also the four SRMB distributions “negative” (8155 cells, $\mu=0.6$, $\sigma=0.175$), 50% (3887 cells, $\mu=0.678$, $\sigma=0.176$), 100% (4892 cells, $\mu=0.689$, $\sigma=0.167$), and “positive” (2609 cells, $\mu=0.711$, $\sigma=0.184$) differ significantly ($p < 0.0001$).

Since the compactness depends on area and perimeter of the cells, the scatter plots also show significant response to the different toxicity stages (Figs. 7 and 8). For visualization the

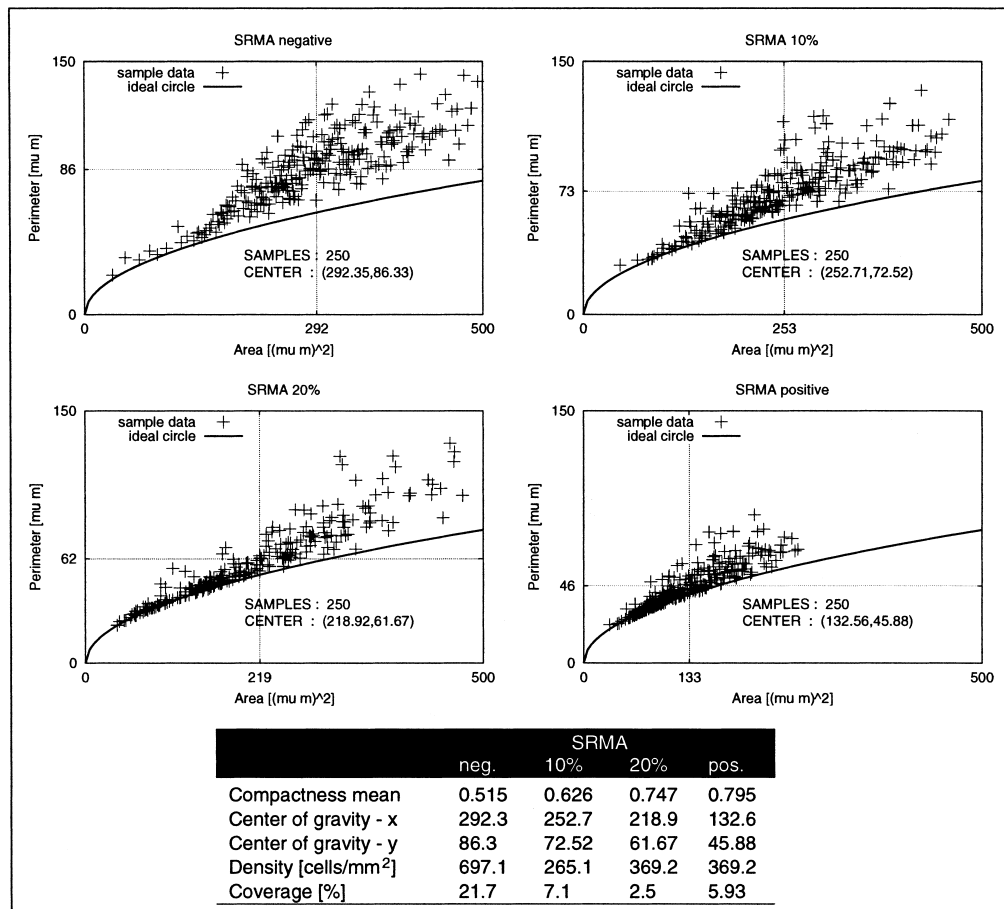


Fig. 7. Cytotoxic effects of SRMA. The negative control (upper left) shows vital cells while SRMA concentrations of 10% (upper right) and 20% (lower left) lead to increasingly deformed cells. The positive control (lower right) shows totally damaged cells. The table depicts extracted parameters.

diagrams are limited to 250 arbitrarily chosen cells. In both cases the normalized measures (mean compactness, mean perimeter, mean area) behave monotonously for increasing toxicities, while the unnormalized measures (cell density, coverage) do not correlate with the toxicity effects (see inserted tables).

4. Discussion

Shape factors specifically designed for certain cytological problems have been presented [31]. Despite the fact that the representation of shape by one parameter is an enormous data compression, there is no optimal single parameter covering all aspects of shape interpretation.

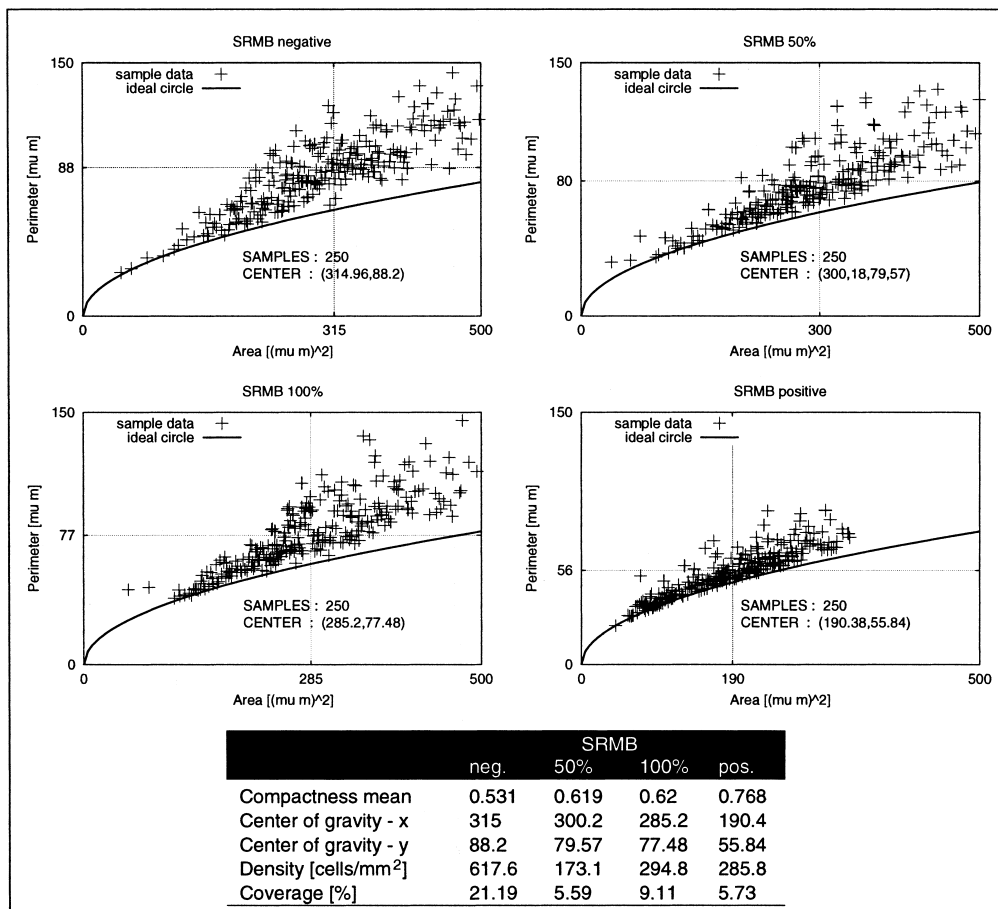


Fig. 8. Cytotoxic effects of SRMB. The diagrams depict the negative control (*upper left*), 50% SRMB (*upper right*), 100% SRMB (*lower left*), and the positive control (*lower right*). Quantitative parameters are given in the table.

Furthermore, the discrimination between different stages of morphological changes, and subsequent evaluation of the toxicity of a biomaterial, leads to a complex classification task. For this reason we utilize only a few characteristic shape parameters, which yield a reasonable discrimination between basic toxicity stages.

The main steps in shape analysis are summarized in Fig. 9. The cytological sample (*upper left*) is first binarized to discriminate objects from background by local adaptive thresholding. At this stage segmentations still contain noise and smaller spurious segments (*upper middle*). Morphological filtering yields binary objects that correspond to cells (*upper right*). Such results can only be achieved with nonlinear filters, because they do not smooth high-frequency object boundaries like linear filters do [32]. The morphological separation yields single cells that are prepared for subsequent quantification (*lower middle*).

Reference results of manual expert segmentation are given in Fig. 9 (*lower right*). Note that all manually determined separations are also found automatically. Moreover, manually segmented cells are generally larger and have a smoother appearance, but do not necessarily improve cell representation. The only obvious advantage of expert segmentation is the acknowledgment of long dendrites.

From these observations we conclude that distributions of shape parameters, acquired from automatically segmented micrographs, are as robust and useful for toxicity evaluation as are manually segmented images. This statement is verified by results enabling unique quantitative discrimination of the cells under toxic influence. The experiments demonstrate the robustness of our method and statistical significance of the normalized parameters, which are independent of the actually used number of cells. The unnormalized parameters depend on the locations of detected cells on the sample, since cell concentrations usually vary heavily due to adhesion effects, especially for high toxicities. It is, therefore, an additional difficulty for manual expert

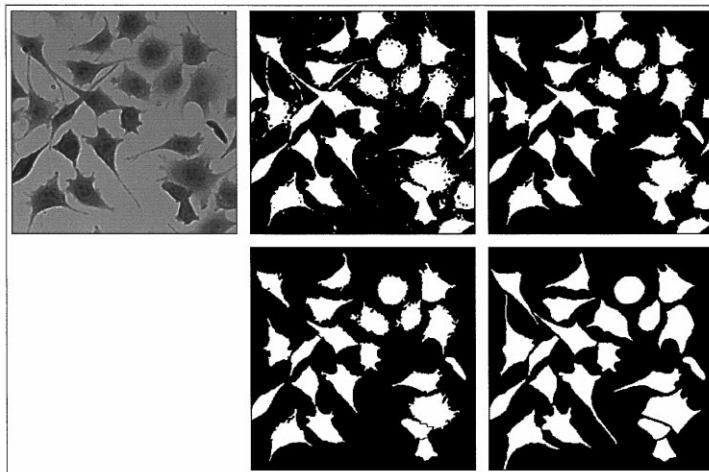


Fig. 9. A micrograph of a cytological sample (microscopic magnification $\times 100$) (*upper left*) is automatically binarized (*upper middle*), filtered (*upper right*), and finally separated (*lower middle*). The manual expert segmentation (*lower right*) yields the same number of cells and preserves dendrites.

segmentation to catch statistically meaningful groups of cells. This favors our computerized method.

The experimentally obtained quantitative data correlate well with the deformation of cells induced by toxic material. Hence, our method accounts for common verbal and qualitative descriptions of morphological cell changes. Population-specific quantitative parameters can be gathered as feature vectors representing points in a multi-dimensional space. Such representations may be subjected to clustering methods to determine thresholds for toxicity of biomaterials.

Since all external control parameters can be estimated from cell sizes, the presented method may be adapted systematically to other monolayered cell populations. Our method is already in use for extensive automatic biocompatibility tests, yielding reproducible data much faster than the usual subjective inspection [17]. At present, we are extending the quantification module towards a multiscale shape representation by calculating the pattern spectra of the populations [33].

5. Summary

Cytotoxicity tests are of vital importance for biocompatibility evaluations of new biomaterials. Morphological changes of cells in contact to those materials indicate their toxicity. In routine applications, however, information on cytotoxic effects is still obtained by subjective visual inspection of microscopic samples. Such qualitative evaluations are user dependent and, for this, limited in their usefulness.

In this paper, a novel computer-assisted method is introduced, which automatically analyses general shape deformations in cell populations and yields reproducible toxicity data. Quantitative shape descriptors are extracted from digitized micrographs in three stages: segmentation, separation, and quantification.

Images are segmented by a novel local adaptive thresholding technique that minimizes the influence of illumination inhomogeneities, by adapting both the window size and the threshold within each window to local graylevel distributions. The method yields minimal windows that contain object and background information. A threshold for each window is obtained by maximizing inter-class variances and minimizing intra-class variances, respectively.

The subsequent scale-independent separation of connected cells cleans the binarized samples from noisy pixels, such as cell compartments and other artifacts, by morphological reconstruction filtering. The cell separation is performed by a two-stage multiscale algorithm. During the analysis stage an image is decomposed into morphological size-specific scales, each of which is carrying separated markers for all cells of that specific size. Since the minimal size of the cells is known a priori, binary noise is removed from each scale by reconstructive filtering. Thereafter, the synthesis stage reconstructs the original cell shapes from these marker scales without merging separated objects.

Subsequent measurement of compactness provides meaningful quantification of shape deformations. Therefore, our method yields reliable evaluations of cytotoxicity of biomaterials.

Our method was evaluated for the standard cell line of fibroblasts in contact to the toxic reference substances ethanol, SRMA, and SMRB. Quantitative parameters obtained for

different toxic concentrations were found to be statistically significant and in excellent agreement with expert descriptions. However, our automatic method has several advantages in comparison to subjective examination. For example, the results permit objective comparisons in a much shorter time. Finally, the method can easily be adapted to further monolayered cell populations via external control parameters depending exclusively on the minimal and maximal size of cells. The method is now in use for extensive cytotoxicity tests of biomaterials.

References

- [1] G.G. Niederauer, T.D. MacGee, J.C. Keller, R.S. Zaharias, Attachment of epithelial cells and fibroblasts to ceramic materials, *Biomaterials* 15 (5) (1994) 342–352.
- [2] J. Sklansky, P.V. Sankar, R.J. Walter Jr, Biomedical image analysis, in: T.Y. Young, K.-S. Fu (Eds.), *Handbook of Pattern Recognition and Image Processing*, Academic Press, San Diego, CA, 1986, pp. 629–647 Chap. 26.
- [3] I.T. Young, Quantitative microscopy, *IEEE Engineering in Medicine and Biology* 15 (1) (1996) 59–66.
- [4] E.R. Dougherty, *An Introduction to Morphological Image Processing*, SPIE Press, Bellingham, WA, 1992.
- [5] P. Soille, *Morphological Image Analysis*, Springer-Verlag, Berlin, 1999.
- [6] P. Maragos, R.W. Schaffer, Morphological filters — Part II: Their relation to median, order-statistic, and stack filters, *IEEE Trans. on Acoustics, Speech, and Signal Processing* 35 (8) (1987) 1170–1184.
- [7] S.-C. Pei, C.-L. Lai, An efficient class of alternating sequential filters in morphology, *Graphical Models and Image Processing* 59 (2) (1997) 109–116.
- [8] F. Meyer, S. Beucher, Morphological segmentation, *Journal of Visual Communication and Image Representation* 1 (1) (1990) 21–46.
- [9] S. Godbole, A. Amin, Mathematical morphology for edge and overlap detection for medical images, *Real-Time Imaging* 1 (1995) 191–201.
- [10] J. Serra, *Image Analysis and Mathematical Morphology*, Academic Press, London, 1982.
- [11] J.C. Russ, *Computer-Assisted Microscopy*, Plenum Press, New York, 1990.
- [12] R.M. Haralick, L.G. Shapiro, Image segmentation techniques, *Computer Vision, Graphic and Image Processing* 29 (1985) 100–132.
- [13] Y.J. Zhang, Evaluation and comparison of different segmentation algorithms, *Pattern Recognition Letters* 18 (1997) 963–974.
- [14] K. Wu, D. Gaultier, M.D. Levine, Live cell image segmentation, *IEEE Trans. on Biomedical Engineering* 42 (1) (1995) 1–12.
- [15] S.H. Ong, X.C. Jin, Jayasooriah, R. Sinniah, Image analysis of tissue sections, *Computers in Biology and Medicine* 26 (3) (1996) 269–279.
- [16] V. Metzler, J. Bredno, T. Lehmann, K. Spitzer, A deformable model for the segmentation of cytological samples, *Proceedings of SPIE* 3338 (1998) 1246–1257.
- [17] V. Metzler, H. Bienert, T. Lehmann, K. Mottaghy, K. Spitzer, A novel method for quantifying shape deformation applied to biocompatibility testing, *ASAIO Journal* 45 (4) (1999) 264–271.
- [18] P. Salembier, M. Kunt, Size-sensitive multiresolution decomposition of images with rank order based filters, *Signal Processing* 27 (1992) 205–241.
- [19] B.K. Jang, R.T. Chin, Morphological scale space for 2D shape smoothing, *Computer Vision and Image Understanding* 70 (2) (1998) 121–141.
- [20] R.C. Gonzales, R.E. Woods, *Digital Image Processing*, Addison-Wesley, Reading, MA, 1993.
- [21] A.V. Oppenheim, R.W. Schafer, T.G. Stockham Jr, Nonlinear filtering of multiplied and convolved signals, *Proceedings of the IEEE* 56 (8) (1968) 1264–1291.
- [22] K. Skifstad, R. Jaim, Illumination independent change detection for real world image sequences, *Computer Vision, Graphics, and Image Processing* 46 (1989) 387–399.

- [23] N. Otsu, A threshold selection method from grey level histograms, *IEEE Trans. on Systems, Man, and Cybernetics* 9 (1979) 62–66.
- [24] J. Crespo, V. Maojo, New results on the theory of morphological filters by reconstruction, *Pattern Recognition* 31 (4) (1998) 419–429.
- [25] C.L. Orbert, E.W. Bengtsson, B.G. Nordin, Watershed segmentation of binary images using distance transformations, *Proceedings of SPIE* 1902 (1992) 159–170.
- [26] G. Borgefors, Distance transforms in digital images, *Computer Vision, Graphics and Image Processing* 34 (1986) 679–698.
- [27] J.D. Banfield, A.E. Raftery, Ice-flow identification in satellite images using mathematical morphology and clustering about principal curves, *Journal of American Statistical Association* 87 (1992) 7–16.
- [28] C.A. Glasbery, G.W. Horgan, *Image Analysis for the Biological Sciences*, Wiley and Sons, Chichester, 1995.
- [29] T. Lehmann, A. Sovakar, W. Schmitt, R. Repges, A comparison of similarity measures for digital subtraction radiography, *Computers in Biology and Medicine* 27 (2) (1997) 151–167.
- [30] T. Tsuchiya, Studies on the standardization of cytotoxicity tests and new standard reference materials useful for evaluating the safety of biomaterials, *Journal of Biomaterial Application* 9 (2) (1994) 138–157.
- [31] C.M. Payne, C.G. Bjorne Jr, D.W. Cromey, F. Roland, A comparative mathematical evaluation of contour irregularity using form factor and PERBAS, a new analytic shape factor, *Analytical and Quantitative Cytology and Histology* 11 (5) (1989) 341–352.
- [32] N.C. Gallagher, G.L. Wise, A theoretic analysis of the properties of median filters, *IEEE Trans. on Acoustics, Speech, and Signal Processing* 29 (1981) 1136–1141.
- [33] P. Maragos, Pattern spectrum and multiscale shape representation, *IEEE Trans. on Pattern Analysis and Machine Intelligence* 11 (7) (1989) 701–716.

Volker Metzler obtained his education in computing at the Imperial College, London, England, and at the Aachen University of Technology, Germany, where he received his Master's degree in 1996. Until 1998 he had been working on stochastic optimization in image processing and quantitative microscopy with the Medical Faculty of the Aachen University. Currently he is research associate with the Institute for Signal Processing of the Medical University of Lübeck, Germany, where he is working in medical image processing. His research interests lie in morphological image processing, scale-space methods, and nonlinear filtering for image segmentation, restoration and quantitative analysis. He is a member of the Institute of Electrical and Electronics Engineers (IEEE) and the Society of Photo-Optical Instrumentation Engineering (SPIE).

Thomas Lehmann earned the Master degree in electrical engineering and the Ph.D. (summa cum laude) in Computer Science from the Aachen University of Technology (RWTH) in 1992 and 1998, respectively. In 1992 he was Research Scientist at the Faculty of Electrical Engineering, RWTH Aachen. Since 1992 he has been with the Institute of Medical Informatics, Medical Faculty, RWTH Aachen, where he currently heads the Department of Medical Image Processing at Assistant Professor level.

In 1993 he was given the DAGM-Preis '93. The award from the German Association for Pattern Recognition was given for his work on automatic strabometry using the Hough transform and covariance filtering. In 1998 he received the Borcher's Medal from the RWTH Aachen for his work on medical image registration. He co-authored a textbook on image processing for the medical sciences, which has been published by Springer-Verlag, Berlin. He is Chairman of the German Workshop on Medical Image Processing and Vice-President of the working group Medical Image Processing within the German Society of Medical Informatics, Biometry and Epidemiology (GMDS).

He is a member of the International Association of Dentomaxillofacial Radiology (IADMFR), the Institute of Electrical and Electronics Engineers (IEEE) and the Society of Photo-Optical Instrumentation Engineering (SPIE). His research interests are discrete realizations of continuous image transforms, medical image processing applied to quantitative measurements for diagnoses and content-based image retrieval from large databases.

Khosrow Mottaghy studied mechanical engineering (Dipl. Ing.) at the Technical University of Munich, Biology (Doctorate) at the Ludwig-Maximilians-University Munich and Medicine (pre-clinical) at the Ruhr-University Bochum. In 1985 he received his habilitation at the Medical Faculty of the Aachen University of Technology (RWTH). Since 1985 he has been Professor for Applied Physiology, at the Department of Physiology, Medical Faculty of the Aachen University of Technology (RWTH). His main subjects in research are hemorheology, respiration physiology, artificial organs and biomaterials. He is a member of the American Society for Artificial Internal Organs, the European Society for Artificial Organs, the German Society of Physiology and the Interdisciplinary Center for Research on Biomaterials (IZKF) Biomater, Aachen.

Klaus Spitzer earned a Masters degree in mathematics and Ph.D. (magna cum laude) in mathematics from the Friedrich-Wilhelms-University, Bonn, in 1983 and 1985, respectively. He earned the M.D. (summa cum laude) from the Friedrich-Wilhelms-University, Bonn, in 1983. From 1983 to 1993 he was physician and neurologist at the Department of Neurology, University Hospital of Hamburg. He was Professor of Neurology at the University of Hamburg from 1992 to 1994, and Associated Professor of Medical Informatics from 1993 to 1995 at the University of Heidelberg. Since 1995 he has been Professor of Medical Informatics and Chair of the Department of Medical Informatics and Biometry at the Aachen University of Technology (RWTH). His research fields are knowledge-based systems in medicine, computer-based training, digital patient records, hospital information systems and management of IT-systems.